CARBON 50 (2012) 3407–3415

Available at www.sciencedirect.com

SciVerse ScienceDirect

journal homepage: www.elsevier.com/locate/carbon

The use of polyethyleneimine-modified reduced graphene oxide as a substrate for silver nanoparticles to produce a material with lower cytotoxicity and long-term antibacterial activity

Xiang Cai [a], *Minsong Lin* [a], *Shaozao Tan* [a,*], *Wenjie Mai* [b], *Yuanming Zhang* [a], *Zhiwen Liang* [b], *Zhidan Lin* [c], *Xiuju Zhang* [c]

[a] *Department of Chemistry, Jinan University, Guangzhou 510632, PR China*
[b] *Department of Physics and Siyuan Laboratory, Jinan University, Guangzhou, Guangdong 510632, PR China*
[c] *Department of Material Science and Engineering, Jinan University, Guangzhou, Guangdong 510632, PR China*

ARTICLE INFO

Article history:
Received 12 December 2011
Accepted 1 February 2012
Available online 9 February 2012

ABSTRACT

In order to improve the stability and decrease the cytotoxicity of silver nanoparticle (AgNP), a polyethyleneimine-modified reduced graphene oxide (PEI-rGO) was used as the substrate of AgNPs, and a PEI-rGO–AgNP hybrid was prepared by anchoring the AgNPs on the reduced graphene oxide surface. Such a hybrid showed substantially higher antibacterial activity than polyvinyl pyrrolidone (PVP)-stabilized AgNP, and the AgNPs on PEI-rGO were more stable than the AgNPs on PVP, resulting in long-term antibacterial effects. The hybrid showed excellent water-solubility and lower cytotoxicity, suggesting the great potential application as a sprayable graphene-based antibacterial solution.

1. Introduction

Silver nanoparticle (AgNP) is well known to be antiseptic to a spectrum of bacteria, and has been increasingly used for their antibacterial properties in detergents, plastics, food storage containers, antiseptic sprays, catheters, bandages and textiles [1,2]. There is a general agreement that the biological action of AgNP, especially pronounced against microorganisms, is derived from the dissolved silver cation (Ag^+) and its soluble complexes [3]. The function of AgNP in these ion-based toxicity pathways is (i) to generate a sustained flux of Ag^+ from an inventory of AgNP bound on substrates or imbedded in matrices or (ii) to transport active Ag^+ to sensitive biological targets on cell membranes or within cells following particle attachment or endocytosis, respectively [4]. On the other hand, AgNP and released Ag^+ have shown cytotoxicity [5]. Some works showed that AgNP was more toxic than Ag^+ [6,7], while others showed the opposite conclusion [8]. Although results from recent studies appear ambiguous, both of the AgNP and released Ag^+ show serious cytotoxicity [5–8]. What is more, practical application of AgNP is often hampered by the aggregation and loss of antibacterial activity [9]. As these facts directly determine the applications of AgNP, and also influence the toxicity of AgNP in humans, it is highly important to control the release of Ag^+ from AgNP and to increase the stability of AgNP. To address these problem, organic [10–16] and inorganic [17] substances have been employed to stabilize AgNP or to control the release of Ag^+, and these strategies can partly enhance the antibacterial activity and stability of AgNP.

Graphene is a single-atom-thick two-dimensional graphitic carbon material [18]. This extremely thin nanomaterial

* *Corresponding author:* Fax: +86 2085 223670.
E-mail address: shaozao@163.com (S. Tan).
0008-6223/$ - see front matter © 2012 Published by Elsevier Ltd.
doi:10.1016/j.carbon.2012.02.002

possesses extraordinary thermal, mechanical, and electrical properties [19], and holds great promises in potential applications, such as nanoelectronics, conductive thin films, supercapacitors, nanosensors and nanomedine [18,20]. Recently, research attention has been drawn towards the antibacterial activity of graphene and its hybrid materials [21–23]. It was reported that reduced graphene oxide (rGO) exhibited strong antibacterial activity [22,24]. The antibacterial activity of rGO was attributed to membrane stress induced by sharp edges of graphene nanosheets, which may result in physical damages on cell membranes, leading to the loss of bacterial membrane integrity and the leakage of RNA [24]. In our previous study, we reported a rGO based antibacterial hybrid combing the advantages of rGO and organic antibacterial agent, displaying excellent antibacterial activity, specific-targeting capability, water-solubility, and mild cytotoxicity [23].

Here, we report the synthesis of a water-soluble polyethyleneimine-rGO–AgNP (PEI-rGO–AgNP) hybrid and demonstrate the excellent stability, long-term antibacterial effect and mild cytotoxicity of this novel nanostructure. The specific benefits of this novel hybrid include (i) dose control to achieve desired antibacterial effects; (ii) dose limitation to avoid eukaryotic toxicity; (iii) control of product lifetime, before dissolution and diffusion end antibacterial activity; (iv) own higher antibacterial activity; (v) sprayable antibacterial solutions.

2. Experimental

2.1. Materials

Polyethyleneimine (PEI) with a molecular weight of 25,000 was purchased from Sigma and used directly. Polyvinyl pyrrolidone (PVP) with a molecular weight of 58,000 was purchased from Jkchemical and used directly. 1-Ethyl-3-(3-dimethylaminopropyl) carbodiimide hydrochloride (EDC·HCl) and N-hydroxy-succinimide (NHS) were purchased from Sigma–Aldrich and used without further purification. Silver nitrate and graphite powders (spectral pure) were purchased from Sinopharm Chemical Reagent Co., Ltd., and were used as received. Mueller–Hinton broth and nutrient agar culture medium were supplied by Huankai Microorganism Co., Ltd. (Guangzhou, China); *Escherichia coli* (*E. coli*) ATCC 8099 and *Staphylococcus aureus* (*S. aureus*) ATCC 6538 were supplied by Guangdong Institute of Microbiology (Guangzhou, China). Thiazolyl blue tetrazolium bromide (MTT) substance was purchased from Sigma–Aldrich (Shanghai, China). Human nasopharyngeal carcinoma CNE1 (CNE1) cells were supplied by Xiangya School of Medicine, Central South University. All other reagents and solvents were obtained from commercial suppliers. All aqueous solutions were prepared with ultrapure water (>18 MΩ) from a Milli-Q Plus system (Millipore).

2.2. Preparation of PEI-rGO–AgNP

Graphene oxide (GO) was prepared by oxidizing natural graphite powder based on a modified Hummers method as originally presented by Kovtyukhova et al. [25,26]. 10 mL of as-prepared GO supernatant (20 mg/mL) was distributed in 40 mL of ultrapure water to obtain a homogeneous, stable dispersion with the aid of ultrasonication in a water bath (KQ218, 60 W), then, 100 mL PEI solution (20 mg/mL), 400 mg EDC·HCl and 240 mg NHS was added, and the pH value of the mixture was adjusted to 6–7. After reaction for 24 h at room temperature, 100 mg silver nitrate was added to the GO dispersion. After 2 h ultrasonication, 4 mL hydrazine monohydrate (50 wt% in water) was added under stiring, and reduced at 30 °C for 0.5 h. After that, 40 mL hydrazine monohydrate (50 wt% in water) was added and reduced at 85 °C for 48 h; a homogeneous green–black dispersion was obtained. The resulting solution was then filtered through a polycarbonate membrane (0.22 μm pore size) and repeatedly washed by ultrapure water. The collected PEI-rGO–AgNP hybrid was redistributed in ultrapure water by ultrasonication in a water bath (KQ218, 60 W) for 15 min. PVP-stabilized AgNP (PVP–AgNP) was prepared by reducing silver nitrate with glucose in the presence of PVP according to Wang et al. [27].

2.3. General characterization

Zeta potential measurements were performed using a Zetasizer nano ZS (Malvern Instruments) and all the aqueous samples were diluted to 0.05 mg/mL before measurements. X-ray Photoelectron Spectroscopy (XPS) profiles were recorded by an ESCALAB 250 X-ray Photoelectron Spectroscopy (Thermo-VG Scientific). Transmission Electron Microscopy (TEM) images were observed by using a JEOL JEM-2100F transmission electron microscope. UV/Vis spectra were recorded by a Hitachi 330 UV–vis spectrophotometer. Atomic Force Microscopy (AFM) images were observed by a Benyuan CSPM5500 atomic force microscope on a flat mica substrate. Fourier Transform Infrared Spectroscopy (FTIR) spectra were obtained on a Nicolet 6700 spectrometer. X-ray Diffraction (XRD) patterns were taken by a Rigaku D/max 2500v/pc X-ray diffractometer using Cu $K\alpha$ radiation ($K\alpha$ = 0.15405 nm) at a scanning rate of 10.0°/min, using a voltage of 40 kV and a current of 200 mA.

2.4. Antibacterial test

The new prepared samples were dispensed into 10 mL of a sterile 0.8 wt% saline water containing about 10^6 cfu/mL of *E. coli* or *S. aureus*, and then shaken at 37 °C. After 6 h contact, 0.1 mL of the suspension was taken out from the test tube and diluted to a certain volume (to ensure the bacterial colonies grown could be counted easily and correctly) by 10-fold dilution. The diluted solution was plated on Luria Bertani broth agar plates in triplicate and incubated at 37 ± 1 °C for 24 h. The killing rate (η) is relative to the viable bacteria counts as follows: $\eta=(Y-X)/Y\times 100\%$, where Y is the number of microorganism colonies on the control tube (a sterile 0.8 wt% saline water without sample) and X is the number of microorganism colonies on the samples. The test was repeated three times.

2.5. Release property

Release property of PEI-rGO–AgNP was tested by dialysis experiments [3]. Dialysis experiments were carried out in dialysis tubes (Spectra/Por Biotech; cellulose ester; MWCO 100,000) filled with 5 mL solution or dispersion and immersed

within 500 mL of ultrapure water. The dialysis was carried out under slow stirring with a magnetic stirrer at 35 °C. The concentration of Ag^+ was measured by an Optima 2000DV Inductively Coupled Plasma optical emission spectrometer (ICP).

2.6. *Cytotoxicity assay*

Cytotoxicity of PEI-rGO–AgNP was tested by using the MTT assay based on the cellular uptake of MTT and its subsequent reduction in the mitochondria of living cells to dark blue

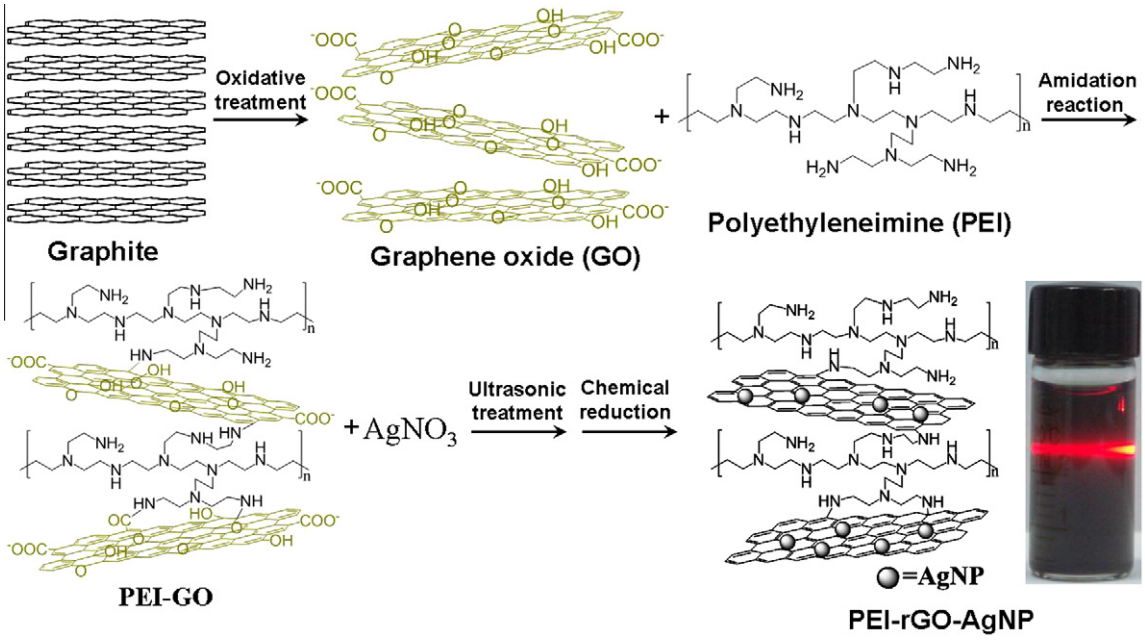

Fig. 1 – The synthesis of a water-soluble PEI-rGO–AgNP hybrid: step 1, oxidative treatment of graphite yields single-layer GO; step 2, the amidation reaction between carboxylic groups of GO and amine group of PEI to synthesize PEI-GO; step 3, the ultrasonic treatment of PEI-GO in the presence of silver nitrate produces a PEI-GO/Ag^+ mixture; step 4, the chemical reduction of GO and silver nitrate with hydrazine monohydrate produces a water-soluble PEI-rGO–AgNP dispersion.

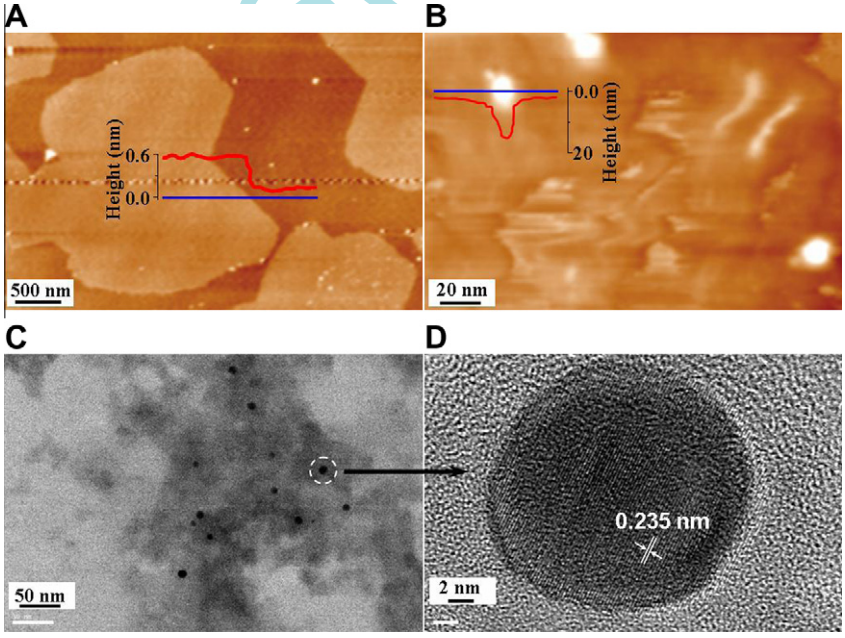

Fig. 2 – (A) Tapping-mode AFM image of PEI-rGO on a clean mica surface and cross-sectional profile of PEI-rGO indicated by a blue line. (B) Tapping-mode AFM image of PEI-rGO–AgNP on a clean mica surface and cross-sectional profile of AgNP indicated by a blue line. (C) TEM images of PEI-rGO–AgNP. (D) HRTEM images of AgNP with fringe spacing. (For interpretation of the references to color in this figure legend, the reader is referred to the web version of this article.)

MTT formazan crystals [28]. CNE1 cells were seeded on 96-well plates ($1.5–2 \times 10^4$ cells/well) in corresponding medium. Then, the cells were treated with the AgNP, PEI modified rGO (PEI-rGO) or PEI-rGO–AgNP for 24 h. After that, MTT (5 mg/mL in PBS) was added to each well and incubated for additional 4 h (37 °C, 5% CO_2). The cells were then lyzed in dimethyl aminoxide (150 μL/well) and the plates were allowed to stay in the incubator (37 °C, 5% CO_2) to dissolve the purple formazan crystals. The color intensity reflecting cell viability was read at 570 nm using a Model-550 Enzyme-linked immunosorbent microplate (Bio-Rad, USA), and the morphologic changes of CNE1 cells were photographed by a IX-70 Olympus inverted phase contrast microscope. All the experiments were repeated four times. Statistical analysis was performed using Statistical Product and Service Solutions software (SPSS) statistical software (SPSS 11.0, United States). The differences between the groups were assessed using the analysis of variance test. The results were considered statistically significant when the *P* value was <0.05 or <0.01.

3. Results and discussion

3.1. *Formation mechanism and water-solubility of PEI-rGO–AgNP*

We have prepared the PEI-rGO–AgNP hybrid by a four-step approach as illustrated in Fig. 1. Under the present experimental conditions, only GO is suitable for the preparation of PEI-rGO–AgNP hybrid. The nucleation of AgNP at GO surfaces should be mainly governed by the presence of oxygen groups at GO which contribute to an overall negatively charged surface, and the overall negatively charged functional groups are responsible for a previous attachment of the free Ag^+ in solution because of electrostatic interactions. Afterward, the addition of the reducing agent to the precursor solution promotes the subsequent reduction of GO and Ag^+, enabling the growth of AgNP at the rGO surface [29]. The dark-blue and homogeneous dispersion (Fig. 1) with concentration up to 1.4 mg/mL was found to remain stable without visible precipitate for more than 3 months.

The thickness of the PEI-GO is ca. 0.6 nm by AFM (Fig. 2A), which is greater than that of single-layer graphene (0.334 nm). The increase in thickness may be attributed to the modified of PEI on the rGO surface. To examine this hypothesis, FTIR of GO, PEI and PEI-rGO are detected. As is observed from FTIR spectrum of GO (Fig. 3), the very broad, intensive peak appeared at 3430 cm^{-1} is assigned to O–H stretching band, which might originate from water adsorbed inside GO. Peaks at 1726, 1622, 1385 and 1052 cm^{-1} correspond to C=O, C–OH, C=C, and C–O–C vibration frequency, respectively. These new peaks suggest that graphite have been oxidized to GO [30,31]. The spectrum of PEI-rGO shows obviously all the PEI absorption features, and the peak at 1668 cm^{-1} is attributed to the O=C–NH stretch. This result confirms that rGO has been covalently modified by PEI successfully. The dispersion of the AgNP on the 2D sheet of PEI-rGO can be visualized in the AFM image in Fig. 2B. The AFM analysis confirms the ability to attain a uniform distribution of 5–15 nm diameters AgNPs anchored on the

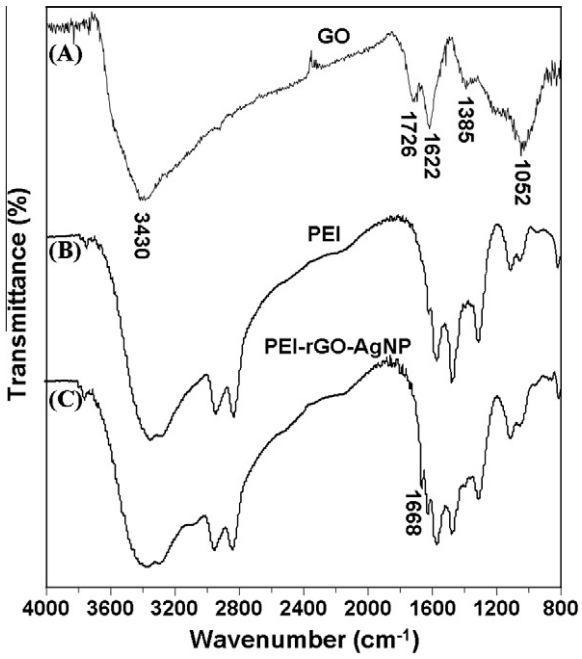

Fig. 3 – FTIR spectra of (A) GO, (B) PEI and (C) PEI-rGO–AgNP.

PEI-rGO nanosheets. The corrugated nature of the PEI-rGO sheets is evident by this analysis.

The TEM micrograph in Fig. 2C further depicts a representative image of PEI-rGO–AgNP. The thin structure of the PEI-rGO–AgNP hybrid and poriferous surface are confirmed. Analysis of the image shows a homogeneous distribution of particles on the surface of the PEI-rGO with particle sizes roughly in the range of 5–15 nm. The measured fringe lattice of AgNP (Fig. 2D) is found to be 0.235 nm which corresponds to the (111) crystal plane of AgNP. Meanwhile, Fig. 4 shows the XPS spectra of the PEI-rGO–AgNP hybrid. The binding energies of 368.8 eV and 374.8 eV were attributed to Ag $3d_{5/2}$ and Ag $3d_{3/2}$, respectively. The 6.0 eV slitting of the 3d doublet of Ag indicates the formation of metallic Ag on the surface of PEI-rGO [32]. What is more, the binding energy of 399.1 eV is attributed to N 1s of PEI, which corresponds to the nitrogen atom in the amino groups of PEI of the PEI-rGO–AgNP.

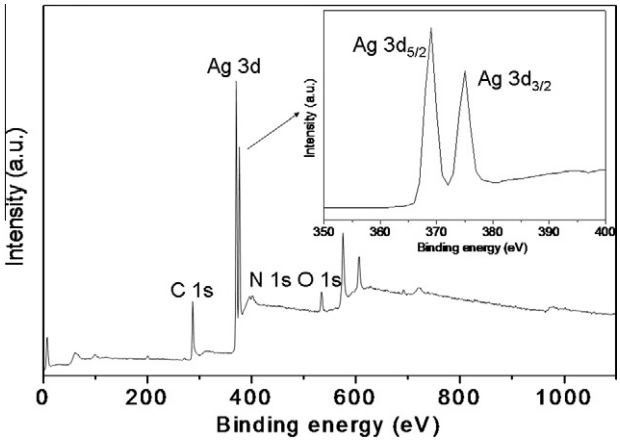

Fig. 4 – XPS profiles of PEI-rGO–AgNP.

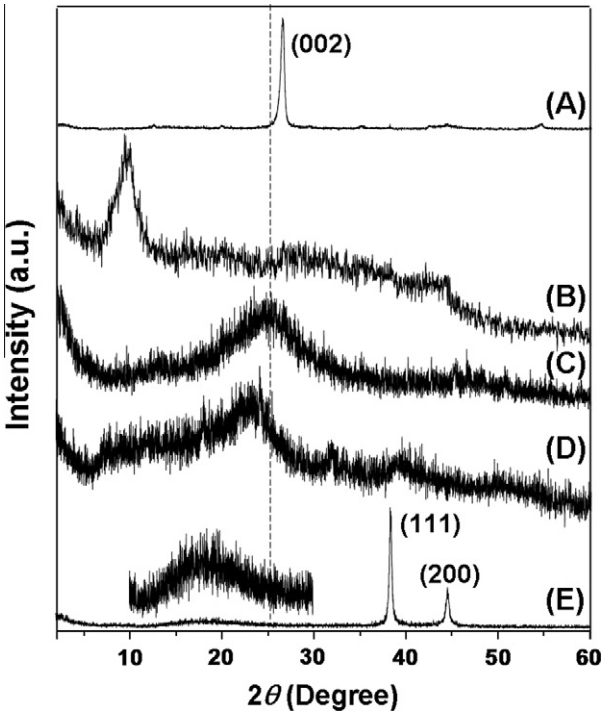

Fig. 5 – XRD patterns of (A) graphite; (B) GO; (C) rGO; (D) PEI-rGO; (E) PEI-rGO–AgNP.

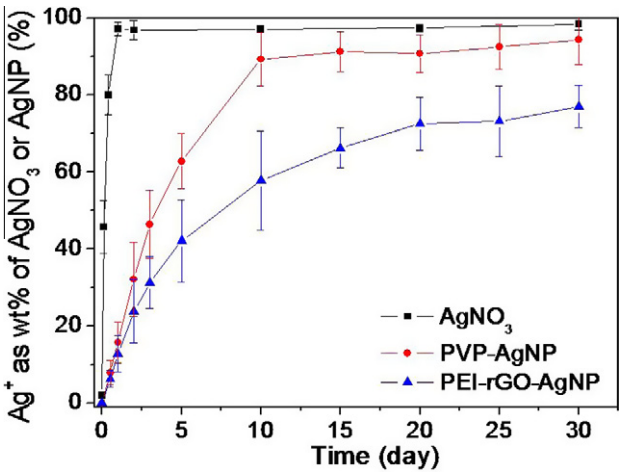

Fig. 6 – Data collected for the dissolution of $AgNO_3$, PVP–AgNP and PEI-rGO–AgNP at 35 °C.

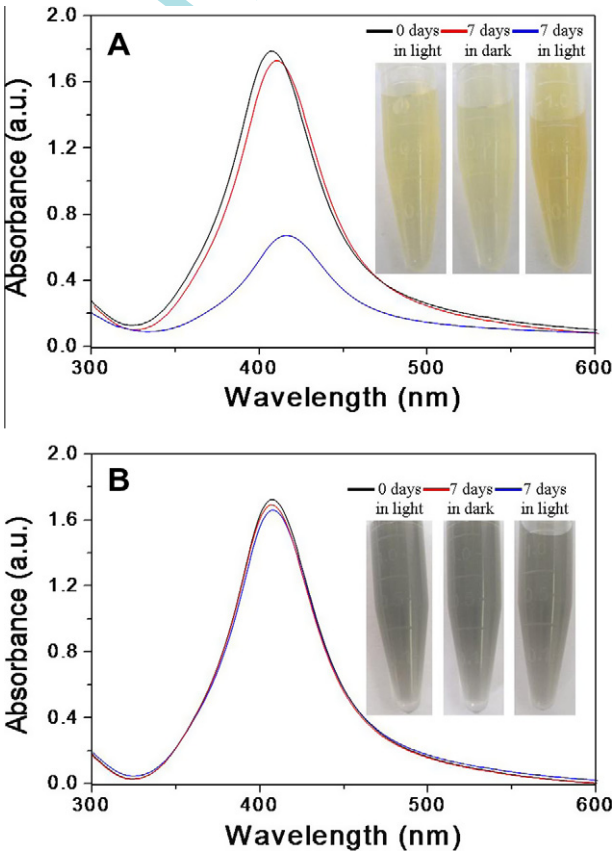

Fig. 7 – Stability comparison of PEI-rGO–AgNP and PVP–AgNP. The absorption spectra of PVP–AgNP (A) and PEI-rGO–AgNP (B) with a surface plasmon resonance band: black line, new synthesis; red line, stored in dark; green line, stored in light. Inset: digital images of the sample under different conditions. (For interpretation of the references to color in this figure legend, the reader is referred to the web version of this article.)

The XRD patterns give the same result. XRD patterns of graphite, GO, rGO, PEI-rGO and PEI-rGO–AgNP were shown in Fig. 5. The low XRD signal-to-noise ratios of GO, rGO and PEI-rGO were attributed to the poor crystallinity of the samples. For graphite, the sharp and intensive peak at $2\theta = 26.4°$ indicated a highly organized crystal structure with the (002) interlayer spacing of 0.337 nm. For GO, the peak at $2\theta = 26.4°$ cannot be observed, and a new peak centered at $2\theta = 9.3°$, corresponding to the (002) interlayer spacing of 0.950 nm, which might be due to high degree of exfoliation and disordered structure of GO. For rGO, the peak at $2\theta = 24.8°$, represented the (002) interlayer spacing of 0.359 nm. This value was slightly larger than that of graphite, which was mainly due to the residual functional groups that may existed between the rGO layers. For PEI-rGO, the diffraction peak shifted even further to $2\theta = 22.9°$, indicating the (002) interlayer spacing of 0.388 nm. This could be explained by the slight broadening of (002) interlayer spacing due to the disturbance of PEI molecules. For PEI-rGO–AgNP, the diffraction peak shifted even further to $2\theta = 18.2°$, indicating the (002) interlayer spacing of 0.487 nm, this can be explained by the slight broadening of (002) interlayer spacing due to the disturbance of PEI and AgNP. Moreover, the sharp and intensive peak at $2\theta = 38.3°$ (111) and $2\theta = 44.2°$ (200) indicated a highly organized crystal structure of AgNPs.

Then, we display the excellent water-solubility of the PEI-rGO–AgNP hybrid. The PEI-rGO–AgNP dispersion showed Tyndall effect (Fig. 1), and a negative Zeta potential of −46.7 mV is found about PEI-rGO–AgNP hybrid in aqueous solution at a concentration around 0.10 mg/mL (pH 7.0, prepared by diluting the purified PEI-rGO–AgNP hybrid in ultrapure water). According to the definition of colloid stability with Zeta potential by the ASTM (American Society for Testing and Materials) Standard D4187-82 [33], the PEI-rGO–AgNP dispersion in the aqueous solution has "good stability" with

Table 1 – The antibacterial activity of the new prepared samples.

Strains	Samples	AgNPs concentrations (mg/L)	PEI-rGO concentrations (mg/L)	The viable colonies of bacteria after contact 6.0 h (cfu/mL)	Killing rate
E. coli	Blank sample	0	0	1.37×10^6	No effect
	PEI-rGO	0	95.8	1.37×10^6	No effect
	PEI-rGO	0	958	$1.14 \sim 1.19 \times 10^6$	14.8 ± 1.7
	PVP-AgNP	4.2	0	$1.48 \sim 1.62 \times 10^5$	86.4 ± 0.6
	PEI-rGO–AgNP	4.2	95.8	$7.95 \sim 9.32 \times 10^4$	93.7 ± 0.5
S. aureus	Blank sample	0	0	1.41×10^6	No effect
	PEI-rGO	0	95.8	1.41×10^6	No effect
	PEI-rGO	0	958	$1.11 \sim 1.13 \times 10^6$	20.5 ± 0.9
	PVP-AgNP	4.2	0	$1.23 \sim 1.82 \times 10^5$	89.2 ± 2.1
	PEI-rGO–AgNP	4.2	95.8	$4.23 \sim 6.77 \times 10^4$	96.1 ± 0.9

Zeta potential values between ±40 and ±60 mV. ICP analysis provides quantitative evidence for the presence of 4.2 mg Ag element L^{-1} in 0.10 mg/mL PEI-rGO–AgNP dispersion, which means the AgNPs content in PEI-rGO–AgNP is 4.2 wt%.

3.2. *The release property and stability of PEI-rGO–AgNP*

According to the previous experiments results, it can be safely assumed that the detected amounts of silver from dialysis experiments are due to only Ag^+ and not AgNPs [3]. As it is obvious from Fig. 6, the diffusion of Ag^+ out of the dialysis tube is very fast and practically completed after a few hours. For PEI-rGO–AgNP and PVP-AgNP, the diffusion of Ag^+ out of the dialysis tube was slow, after 20 days, nearly 72.5% and 90.7% Ag^+ out of the dialysis, respectively. As the PEI-rGO–AgNP shows lower release speed than PVP-AgNP, we would expect the PEI-rGO–AgNP hybrid shows long-term antibacterial effect than that of PVP-AgNP. The majority of Ag^+ comes from oxidation of the zerovalent AgNPs, typically by reaction with dissolved O_2 and mediated by protons and other components in the surrounding fluid phase [Eqs. (1) and (2)] [34].

$$\mathrm{AgNPs} + \mathrm{O_2} \rightarrow \mathrm{AgNPs}\cdots\mathrm{O_2} \xrightarrow{\mathrm{H^+}} \mathrm{Ag^+} + \text{reactive oxygen intermediates} \quad (1)$$

$$\text{reactive oxygen intermediates} + \mathrm{AgNPs} \xrightarrow{\mathrm{H^+}} \mathrm{Ag^+} + \mathrm{H_2O} \quad (2)$$

Methods that disrupt oxidation pathways are promising routs to slow the release of Ag^+ from AgNP surfaces. Many AgNPs formulations use macromolecular coatings, such as dextran [11], starch [12], gum arabic [13], or synthetic polymers [14], which can block oxygen access [15]. We observe here that rGO can more efficient to delay and extend Ag^+ release from AgNPs than PVP.

We also find that the PEI-rGO–AgNP hybrid is more stable than PVP-AgNP. PVP-AgNP are easily aggregated in air, which usually leads to significant reduction of antibacterial activity [35,36]. Corresponding UV–vis spectra show that the absorption peak at 408 nm (PVP-AgNP) shifts to 419 nm with a large decrease in intensity, suggesting aggregation of AgNPs (Fig. 7A) [37,38]. In comparison, the UV–vis spectra of the PEI-rGO–AgNP change little when stored either in dark or light for 7 days (Fig. 7B). Therefore, the PEI-rGO–AgNP is much more stable and resistant to aggregation than PVP-AgNP. The high stability of AgNPs at the surface of the rGO anchors the AgNPs to the surface and prevented their aggregation. Since the nanoparticle suspensions will be exposed to environmental conditions different from a research lab setting, many factors, including light, temperature, salinity, etc., are suspected to affect the stability of the nanoparticle. So, the high stability of PEI-rGO–AgNP is very important for the use of the antibacterial material in environmental conditions. Given the release property and aggregation states of PVP-AgNP, we conclude that the long-term antibacterial activity and high stability of the PEI-rGO–AgNP hybrid is responsible for their practical application.

3.3. *The antibacterial activity of PEI-rGO–AgNP*

Table 1 shows the antibacterial activity of PEI-rGO, PVP-AgNP and PEI-rGO–AgNP after 6 h contact with bacterial. Under lower concentration (95.8 mg/L), PEI-rGO shows no antibacterial activity, because the viable colonies of *E. coli* or *S. aureus* remain essentially unchanged, while the concentration of PEI-rGO reach to 958 mg/L, the killing rate against *E. coli* and *S. aureus* is 14.8% and 20.5%, respectively. It is shown that the antibacterial activity is enhanced when AgNPs are deposited on the PEI-rGO surface, but it does not mean that the antibacterial activity was simple the adding of the antibacterial activity of PEI-rGO and AgNPs. However, the PEI-rGO–AgNP hybrid

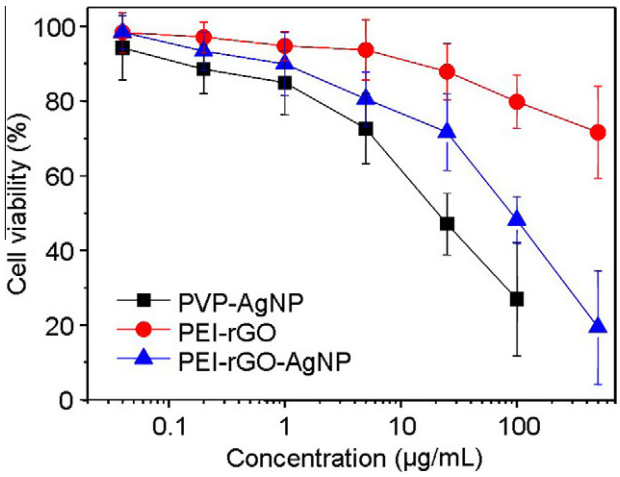

Fig. 8 – Cytotoxicity of PVP–AgNP, PEI-rGO and PEI-rGO–AgNP on CNE1 cells.

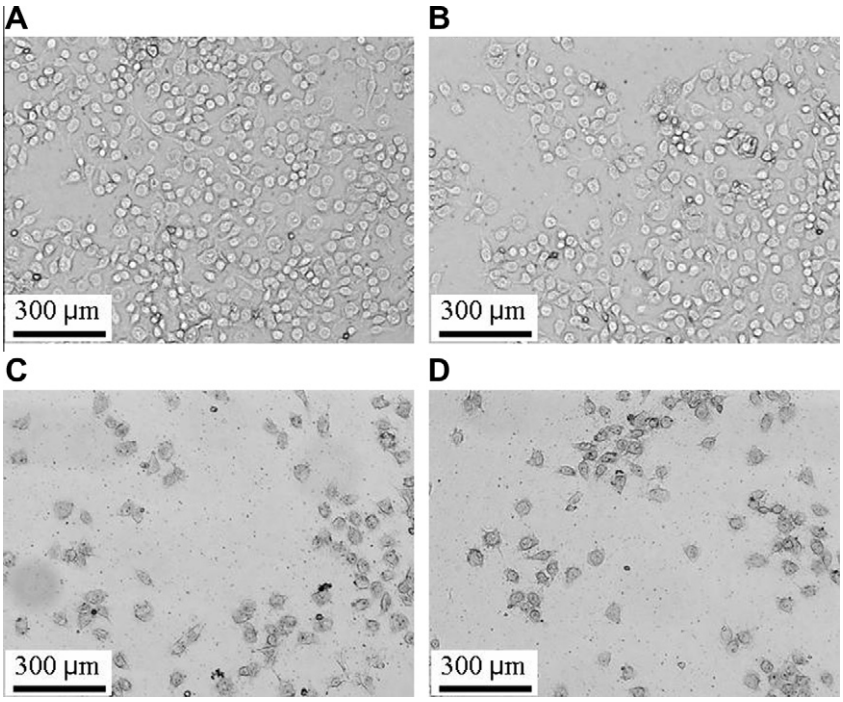

Fig. 9 – Morphologic changes of CNE1 cells in control group and experimental groups. (A) In the control group, the CNE1 cells had good shape, presented long fusiform or polygon. The presence of round dividing cells showed their vigorous growth. (B) The CNE1 cells shape became irregular when the concentration of PEI-rGO was set at 500 μg/mL after 24 h. (C) The CNE1 cells shape became more irregular, and the shapes of majority of the cells were injured, when the concentration of PEI-rGO–AgNP hybrid was set at 500 μg/mL after 24 h. (D) The number of CNE1 cells decreased significantly, and the shapes of majority of the cells were seriously injured, when the concentration of PVP–AgNP was set at 500 μg/mL after 24 h.

shows obvious higher antibacterial effect than PVP-AgNP. We suggesting the "blade like edges" of PEI-rGO–AgNP can damage the bacterial cell [23], which will made the Ag^+ more quickly and conveniently to react with cytoplasmic constituents, and eventually kill the bacteria. So, the PEI-rGO–AgNP hybrid combines the advantages of both graphene and Ag^+ on antibacterial activity, rendering the Ag^+ more efficient act with bacterial, and the use of AgNP will be more efficient. What is more, compared to Gram-positive species (*S. aureus*), Gram-negative strain (*E. coli*) has an outer membrane outside the peptidoglycan layer, which is composed mainly of lipopolysaccharides and phospholipids. The outer membrane takes a significant role to protect the bacteria cell from attack by foreign compounds. So, all samples show lower antibacterial activity towards *E. coli* [39,40].

3.4. *The cytotoxicity of PEI-rGO–AgNP*

We also carry out cytotoxicity test on the as-synthesized PVP-AgNP, PEI-rGO and PEI-rGO–AgNP. The MTT assays show (Fig. 8) that PEI-rGO (25 μg/mL) exhibits a slight cytotoxicity (~12%) to CNE1 within 24 h incubation. For PVP-AgNP, the cell viability of CNE1 is reduced to 47% and 27% with PVP-AgNP of 25 and 100 μg/mL. However, the cell viability of CNE1 is increased to 72% and 48% with PEI-rGO–AgNP of 25 and 100 μg/mL, respectively. Therefore, the cytotoxicity of PEI-rGO–AgNP is slightly lower than PVP-AgNP, the result is in accordance with the result of inverted phase contrast microscope measurements (Fig. 9). Such difference in cytotoxicity might arise from the different functional groups and the different surface charges of PVP-AgNP and PEI-rGO–AgNP surfaces [22]. Comparing with other report [41], we conclude that PEI-rGO–AgNP hybrid is relatively biocompatible nanomaterials with mild cytotoxicity.

4. Conclusions

We described a PEI-rGO–AgNP hybrid which was prepared by using PEI-rGO as the substrate of AgNPs. Firstly, the PEI-rGO–AgNP hybrid showed excellent water-solubility. With negative Zeta potential of 46.7 mV, the PEI-rGO–AgNP dispersion was found to remain stable for more than 3 months without visible precipitate. The solubility of PEI-rGO–AgNP could reach up to 1.4 mg/mL, and the AgNPs content in PEI-rGO–AgNP was 4.2 wt%. Secondly, the PEI-rGO–AgNP showed excellent stability. The high stability of AgNPs at the surface of the rGO anchored the AgNPs to the surface and prevented their aggregation. Thirdly, the PEI-rGO–AgNP hybrid showed long-term antibacterial effect. The rGO could more efficient to delay and extend Ag^+ release from AgNP than PVP, and the PEI-rGO–AgNP showed long-term antibacterial effect than that of PVP-AgNP. The PEI-rGO–AgNP showed obvious higher antibacterial effect than PVP-AgNP, suggesting the "blade like edges" of PEI-rGO–AgNP could damage the bacterial cell which would make the Ag^+ more quickly and conveniently to react with cytoplasmic constituents, and eventually kill the bacteria. Fourthly, the PEI-rGO–AgNP hybrid was relatively

biocompatible nanomaterials with mild cytotoxicity. Given these advantages, we expect that the PEI-rGO–AgNP hybrid is a promising graphene-based antibacterial material for environmental application.

Acknowledgements

We would like to thank the National Natural Science Foundation of China (21006038, 51172099, 20871058 and 21176100), the Natural Science key Foundation of Guangdong Province of China (10251007002000000), and the Fundamental Research Funds for the Central Universities (21610102).

REFERENCES

[1] Benn TM, Westerhoff P. Nanoparticle silver released into water from commercially available sock fabrics. Environ Sci Technol 2008;42:4133–9.
[2] Blaser SA, Scheringer M, MacLeod M, Hungerbuhler K. Estimation of cumulative aquatic exposure and risk due to silver: contribution of nano-functionalized plastics and textiles. Sci Total Environ 2008;390:396–409.
[3] Kittler S, Greulich C, Diendorf J, Köller M, Epple M. Toxicity of silver nanoparticles increase during storage because of slow dissolution under release of silver ions. Chem Mater 2010;22:4548–54.
[4] Liu J, Sonshine DA, Shervani S, Hurt RH. Controlled release of biologically active silver from nanosilver surfaces. ACS Nano 2010;4:6903–13.
[5] Ahamed M, AlSalhi MS, Siddiqui MKJ. Silver nanoparticle applications and human health. Clin Chim Acta 2010;411:1841–8.
[6] Greulich C, Kittler S, Epple M, Muhr G, Köller M. Studies on the biocompatibility and the interaction of silver nanoparticles with human mesenchymal stem cells (hMSCs). Langenbecks Arch Surg 2009;394:495–502.
[7] Kittler S, Greulich C, Köller M, Epple M. Synthesis of PVP-coated silver nanoparticles and their biological activity towards human mesenchymal stem cells. Materialwiss Werkstofftech 2009;40:258–64.
[8] Asharani PV, Wu YL, Gong Z, Valiyaveettil S. Toxicity of silver nanoparticles in zebrafish models. Nanotechnology 2008;19:255102.
[9] Kong H, Jang J. Antibacterial properties of novel poly(methyl methacrylate) nanofiber containing silver nanoparticles. Langmuir 2008;24:2051–6.
[10] Wu KH, Liu CI, Yang CC, Wang GP, Chao CM. Preparation and characterization of aminosilane-modified silicate supported with silver for antibacterial behavior. Mater Chem Phys 2011;125:802–6.
[11] Ma Y, Yi J, Zhang LA. A facile approach to incorporate silver nanoparticles into dextran-based hydrogels for antibacterial and catalytical applications. J Macromol Sci Part A 2009;46:643–8.
[12] Asharani PV, Mun GLK, Hande MP, Valiyaveettil S. Cytotoxicity and genotoxicity of silver nanoparticles in human cells. ACS Nano 2009;3:279–90.
[13] Rao YN, Banerjee D, Datta A, Das SK, Guin R, Saha A. Gamma irradiation route to synthesis of highly re-dispersible natural polymer capped silver nanoparticles. Radiat Phys Chem 2010;79:1240–6.
[14] Chen M, Wang L, Han J, Zhang J, Li Z, Qian D. Preparation and study of polyacryamide stabilized silver nanoparticles through one-pot process. J Phys Chem B 2006;110:11224–31.
[15] Grubbs RB. Roles of polymer ligands in nanoparticle stabilization. Polym Rev 2007;47:197–215.
[16] Zan X, Kozlov M, McCarthy TJ, Su Z. Covalently attached, silver-doped poly(vinyl alcohol) hydrogel films on poly(l-lactic acid). Biomacromolecules 2010;11:1082–8.
[17] Lv M, Su S, He Y, Huang Q, Hu W, Li D, et al. Long-term antimicrobial effect of silicon nanowires decorated with silver nanoparticles. Adv Mater 2010;22:5463–7.
[18] Geim AK, Novoselov KS. The rise of graphene. Nat Mater 2007;6:183–91.
[19] Matthew JA, Vincent CT, Richard BK. Honeycomb carbon: a review of graphene. Chem Rev 2010;110:132–45.
[20] Yang K, Zhang S, Zhang G, Sun X, Lee ST, Liu Z. Graphene in mice: ultrahigh in vivo tumor uptake and efficient photothermal therapy. Nano Lett 2010;10:3318–23.
[21] Shen J, Shi M, Li N, Ma H, Ye M. Facile synthesis and application of Ag-chemically converted graphene nanocomposite. Nano Res 2010;3:339–49.
[22] Hu W, Peng C, Luo W, Lv M, Li X, Li D, et al. Graphene-based antibacterial paper. ACS Nano 2010;4:4317–23.
[23] Cai X, Tan S, Lin M, Xie A, Mai W, Zhang X, et al. Synergistic antibacterial brilliant blue/reduced graphene oxide/quaternary phosphonium salt composite with excellent water-solubility and specific-targeting capability. Langmuir 2011;27:7828–35.
[24] Akhavan O, Ghaderi E. Toxicity of graphene and graphene oxide nanowalls against bacteria. ACS Nano 2010;4:5731–6.
[25] Hummers WS, Offeman RE. Preparation of graphitic oxide. J Am Chem Soc 1958;80:1339.
[26] Kovtyukhova NI, Ollivier PJ, Martin BR, Mallouk TE, Chizhik SA, Buzaneva EV, et al. Layer-by-layer assembly of ultrathin composite films from micron-sized graphite oxide sheets and polycations. Chem Mater 1999;11:771–8.
[27] Wang H, Qiao X, Chen J, Ding S. Preparation of silver nanoparticles by chemical reduction method. Colloids Surf A 2005;256:111–5.
[28] Yang YH, Dai GJ, Tan SZ, Liu YL, Shi QS, Ouyang YS. Structure and synergetic antibacterial effect of zinc and cerium carried sodium zirconium phosphates. J Rare Earth 2011;29:308–12.
[29] Goncalves G, Marques PAAP, Granadeiro CM, Nogueira HIS, Singh MK, Grácio J. Surface modification of graphene nanosheets with gold nanoparticles. Chem Mater 2009;21:4796–802.
[30] Jeong HK, Lee YP, Lahaye RJ, Park MH, An KH, Kim IJ, et al. Evidence of graphitic AB stacking order of graphite oxides. J Am Chem Soc 2008;130:1362–6.
[31] Guo HL, Wang XF, Qian QY, Wang FB, Xia XH. A green approach to the synthesis of graphene nanosheets. ACS Nano 2009;3:2653–9.
[32] Liu Y, Wang X, Yang F, Yang X. Excellent antimicrobial properties of mesoporous anatase TiO_2 and Ag/TiO_2 composite films. Micropor Mesopor Mater 2008;114:431–9.
[33] American Society for Testing and Materials. Zeta potential of colloids in water and waste water. ASTM Standard D4187-82, 1985.
[34] Liu J, Hurt RH. Ion release kinetics and particle persistence in aqueous nano-silver colloids. Environ Sci Technol 2010;44:2169–75.
[35] Henglein A. Colloidal silver nanoparticles: photochemical preparation and interaction with O_2, CCl_4, and some metal ions. Chem Mater 1998;10:444–50.
[36] Lok CN, Ho CM, Chen R, He QY, Yu WY, Sun H, et al. Silver nanoparticles: partial oxidation and antibacterial activities. J Biol Inorg Chem 2007;12:527–34.

[37] Li X, Zhang J, Xu W, Jia H, Wang X, Yang B, et al. The mercaptoacetic acid-capped silver nanoparticles colloid–formation, morphology and SERS activity. Langmuir 2003;19:4285–90.
[38] Shi Z, Neoh KG, Kang ET. Surface-grafted viologen for precipitation of silver nanoparticles and their combined bactericidal activities. Langmuir 2004;20:6847–52.
[39] Tan SZ, Zhang KH, Zhang LL, Xie YS, Liu YL. Preparation and characterization of the antibacterial Zn^{2+} or/and Ce^{3+} loaded montmorillonites. Chin J Chem 2008;26:865–9.
[40] Hu W, Peng C, Luo W, Lv M, Li X, Li D, et al. Graphene-based antibacterial paper. ACS Nano 2010;7:4317–23.
[41] Ceckova M, Vackova Z, Radilova H, Libra A, Buncek M, Staud F. Effect of ABCG2 on cytotoxicity of platinum drugs: interference of EGFP. Toxicol In Vitro 2008;22:1846–52.